On the Fundamental Limitations of Artificial Magnetic Materials

Ali Kabiri, Leila Yousefi, and Omar M. Ramahi, *Fellow, IEEE*

***Abstract*—Fundamental limitations are presented on the performance of artificial magnetic materials based on the geometrical and physical characteristics of the inclusions comprising the medium. The permeability and magnetic susceptibility of the medium are formulated in terms of newly defined geometrical and physical parameters. Based on the Lorentzian form of the effective permeability function of the medium, it is shown that the flatness of the permeability function is limited by the desired operational bandwidth. Also, by applying a specific circuit-based model for inclusions, geometric invariant fundamental constraints are derived. It is shown that inclusions with larger surface area result in higher value of permeability. Next, the magnetic loss tangent in the medium is expressed as a function of the newly defined geometrical and physical parameters. It is found that there is a tradeoff between increasing the permeability and decreasing the loss on the one hand and reducing dispersion, on the other hand.**

***Index Terms*—Artificial magnetic material, electrically small resonators, magnetic loss tangent, magnetodielectric, metamaterial.**

I. Introduction

In MICROWAVE and sub-microwave frequencies, naturally-occurring materials are limited to certain levels of polarization and magnetization. Even if certain levels of magnetization and polarization are achievable, however, the materials suffer from high electric and magnetic loss. For example, ferrite composites are strongly magnetized yet they suffer from appreciable magnetic loss and high resistivity in the microwave frequency range [1], [2]. Due to these limitations, artificially engineered materials, also referred to as metamaterials, are designed to provide specific permeability and permittivity over microwave frequency ranges [3]–[6]. Artificial magnetic media (AMM), which are produced by an ensemble of small metallic looped inclusions organized periodically or aperiodically, exhibit magnetic behavior when exposed to an applied electromagnetic field.

To obtain enhanced magnetic properties, different inclusions have been proposed having various geometrical configurations [4]–[6]. Each proposed structure provides its own advantages and disadvantages in terms of resultant permeability, dispersive characteristics and dissipation factor. The single and coupled split-ring resonators (SRR), the modified split-ring resonators (MSRR), and the "Swiss Roll" resonators (SR-R) are among popular configurations. In [5], a new configuration named meta-solenoid was proposed with the potential to provide higher permeability compared to SRR and MSRR configurations. In [7], the n-turn spiral resonator (n-SR) configuration was introduced, and in [8] new inclusions based on fractal Hilbert curves were proposed to reduce the size of inclusions.

A number of analytical models were developed to explicate the physics behind the peculiar characteristics of AMMs [4], [6], [9], [10]. When the periodicity and the size of the inclusions are small compared to the wavelength, electromagnetic mixing formulas such effective medium theory (EMT) and homogenization theories (HT) can be used to derive the effective permeability and permittivity for composite media [11]. Using the EMT technique, Pendry *et al.* calculated the effective permeability of a medium containing looped metallic inclusions such as metal cylinders, Swiss Rolls, and SRRs and showed that negative permeability can be obtained in microwave frequencies [4]. EMT allows identifying the average field propagating inside a composite medium with respect to the field propagating inside a homogeneous medium with the same effective electrical characteristic [12].

The circuit-based models of metamaterials, especially artificial magnetic materials, have been developed to capture either the behavior of the entire composite medium or the behavior of the separate inclusions [5]. These models, which depend on the geometry and dimension of the inclusions, have been proposed to describe the magnetic behavior of the inclusions rather than the electric behavior.

Different shapes of inclusions have been studied in the literature. The SRR consists of two concentric metallic broken rings printed on a dielectric circuit board. Marques *et al.* presented a quasi-static study of the SRR by proposing a circuit model for the capacitive behavior of the inclusions [6]. Sauviac *et al.* and Shamonin *et al.* proposed more accurate models for SRR inclusions [9], [13]. Sauviac *et al.* used a detailed circuit-based model to extract the magnetic and electric polarization of the SRR [9]. Shamonin *et al.* expanded a set of differential equations describing the current and voltage distribution in SRRs [13]. Most recently, Ikonen *et al.* offered a generalized equivalent-circuit model which mimics the experimental permeability function [14].

The unique properties of metamaterials have encouraged researchers to use metamaterial slabs in various microwave applications including using metamaterials as a substrate or a superstrate for enhancing low-profile antenna performance [15], [16], as a probe for the near-field imaging [17], or for shielding

Manuscript received January 30, 2009; revised January 04, 2010; accepted January 23, 2010. Date of publication April 22, 2010; date of current version July 08, 2010. This work was supported in part by Research in Motion and in part by the National Science and Engineering Research Council Canada under the NSERC/RIM Industrial Research Chair Program.

The authors are with the Department of Electrical and Computer Engineering, University of Waterloo, Waterloo, ON N2L 3G1, Canada (e-mail: oramahi@ece.uwaterloo.ca).

Color versions of one or more of the figures in this paper are available online at http://ieeexplore.ieee.org.

Digital Object Identifier 10.1109/TAP.2010.2048845

0018-926X/$26.00 © 2010 IEEE

Authorized licensed use limited to: University of Waterloo. Downloaded on July 21,2010 at 14:45:05 UTC from IEEE Xplore. Restrictions apply.

applications and microwave absorbers [18]–[20]. In [15], extensive research was done on the performance of developed engineered magnetic materials when used for antenna miniaturization. It was shown in [8] that new inclusions can provide lower dispersion, nevertheless, high magnetic losses persist. In [21], the effective properties of the medium are expressed in terms of the Q-factor. It was claimed that by measuring the Q-factor of a single fabricated SRR, the effective permeability and permittivity of an AMM can be estimated to better than 20% accuracy. In addition, in [21], a lower limit for the magnetic loss tangent was proposed for frequencies up to about 1 GHz.

This work aims to establish a relationship between the design specification of inclusions and the performance features of artificially engineered magnetic materials. The parameters that play a role in the effective permeability and its variation with respect to frequency are classified into *physical* and *geometrical* variables. Physical variables are parameters which are restricted to (a) fabrication techniques such as the width and height of the printed conductor on the board (i.e., trace), (b) structural characteristics such as space between parallel printed lines, the entire size of structure and its unit cells, and (c) electrical or material characteristics such as conductivity of the conductor and the permittivity of the host medium. Geometrical parameters, on the other hand, include the inclusion's shape and a contour's perimeter, area and curvature. In this work, we derive a general relationship which relates the effective permeability of the structure to the physical and geometrical variables of the inclusion. Moreover, we study the sensitivity of an AMM's magnetic properties such as the permeability function, the magnetic loss tangent (MLT) and dispersion with respect to variation of the geometrical and physical parameters.

In this work, a circuit-based model is used for calculating the magnetic behavior of inclusions and the slab itself. The circuit model developed considers the capacitance between the pairs, ohmic resistance of the inclusions and the inductance created due to the circulating current excited on the inclusions. Although more elaborate models proposed in literature [9], [14] consider more circuit components such as the capacitance of the inclusions gap, inductance of the metallic routes and mutual induction between adjacent inclusions, it has been shown that the general functionality of the effective magnetic behavior of inclusions will not change [4], [5]. Thus, our derivations and conclusions, in essence, are general, and they can be applied for any application and design. It is worth noting that in this work, we only considered the magnetic loss, however, the total loss in the medium can be comprised of electric and magnetic losses.

This paper is organized as follows: In Section II, a general circuit-based model is developed to calculate the effective permeability of inclusions. In Section III, an explicit relationship is derived to connect the deviation in the relative permeability to the relative bandwidth of the artificial magnetic medium, thus predicting a fundamental restriction on the operational bandwidth based on the permissible variation in the permeability. It is shown that the achieved restriction is general and does not depend on the shape of the metallic inclusions. In Section IV, the effect of the geometrical and physical parameters on the permeability and its variation with respect to frequency is studied. Section V provides concluding remarks.

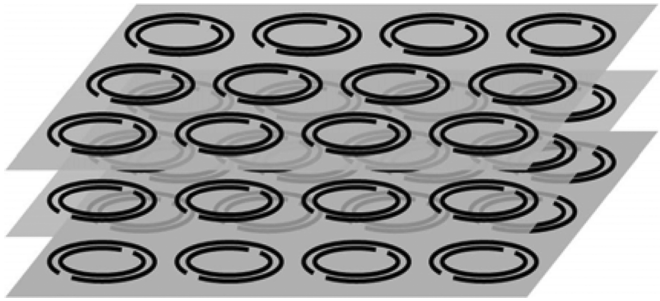

Fig. 1. A metamaterial slab (an artificial composite of metallic inclusions).

II. Problem Formulation

Various geometrical patterns have been proposed to develop artificial magnetic materials [4]–[6]. The key idea to produce magnetic properties is to generate a circulating electric current that mimics a magnetic dipole. The current circulation occurs in a metallic contour leading to increased magnetic flux. To generate a *capacitive* property, another metallic contour is positioned adjacent to the first contour. The coupling between the two contours creates capacitance between them leading to a net effective increase in the permeability. The resultant capacitance and inductance create the potential for resonance at a certain frequency, henceforth referred to as the *resonance frequency*.

Fig. 1 shows an artificial magnetic medium composed of periodic unit cells of generic rings. The ring resonator in a unit cell can be an n-turn spiral or multiple split rings. The rings provide different coupling schemes, namely *edge-coupled* if the rings are concentric in a plane, and *broadside-coupled* if the rings are parallel along their axes. Fig. 2(a) shows a two-turn spiral ring resonator, Fig. 2(b) shows split ring resonators which are edge-coupled, and Fig. 2(c) shows split ring resonators which are broadside-coupled. Fig. 2(e) and Fig. 2(f) show a cross section of edge-coupled and broadside-coupled ring resonators, respectively. The artificial magnetic medium is then created by reproducing the contour in a periodic fashion, infinitely spread along the x, y, and z axes.

The unit samples in Fig. 2 have the height of δz width of δx and depth of δy. The area of each cell is $A = \delta x \delta z$, and its volume is $V = A\delta y = \delta x \delta y \delta z$. The area and circumference of the contours are denoted by s and l, respectively. The conductor material used in printed inclusions is assumed to have electric conductivity of σ, width of b, and height of t. Without loss of generality, we assume the other (twin) conductor is positioned either to the inside and follow the shape of the outer conductor with the uniform gap g (see Fig. 2(e)) or parallel to the former and separated by a distance of g (see Fig. 2(f)).

When an external monochromatic magnetic field $\mathbf{H}_{\rm ext}$ is applied, it induces a circulating current on the metallic inclusion. As a consequence, an induced magnetic field $\mathbf{H}_{\rm ind}$ develops. Based on Faraday's law an electromotive force, $V_{\rm emf}$, develops on the metallic rings given by

$$V_{\rm emf} = -j\omega\mu_0 ns(H_{\rm ext} + H_{\rm ind}) \tag{1}$$

$$H_{\rm ind} = \frac{nI}{\delta y} \tag{2}$$

Authorized licensed use limited to: University of Waterloo. Downloaded on July 21,2010 at 14:45:05 UTC from IEEE Xplore. Restrictions apply.

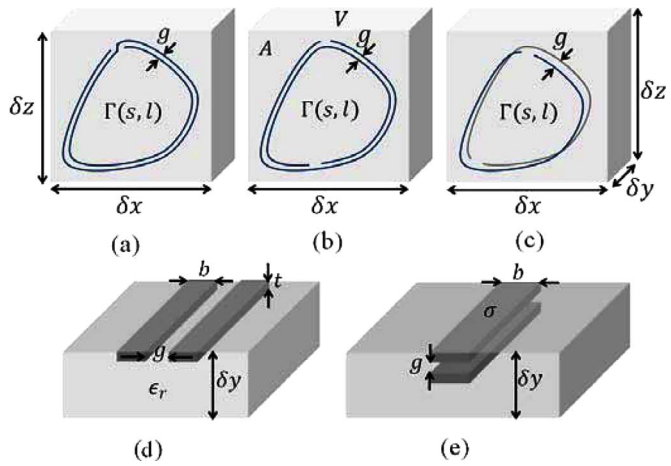

Fig. 2. Configuration of a unit cell of an artificial magnetic material with arbitrary shape of the inclusion. The inclusions' contour, area and perimeter are denoted by Γ, s, and l, respectively. However, V and A represent the volume and surface area of the unit cell. (a) Two-turn spiral inclusion, (b) edge-coupled double split ring resonator, (c) broadside-coupled double modified split ring resonator, (d) a cross section of an edge-coupled inclusion, (e) a cross section of a broadside-coupled inclusion.

where $H_{\rm ind}$ and $H_{\rm ext}$ are the magnitude of the vectors $\mathbf{H}_{\rm ind}$ and $\mathbf{H}_{\rm ext}$, respectively, I is the induced current, n is the number of wire turns that carries the induced current ($n = 2$ for Fig. 2(a) [16], and $n = 1$ for Figs. 2(b) and (c)) [5], ω is the frequency of the applied external field, and μ_0 is the permeability of air. The inclusions are also distributed in the y-direction (along their axis), and, thus, the produced magnetic field in each column passes through the other inclusions of the same stack. For evaluating the magnetic field, δy is considered to be smaller than the largest dimension of the inclusion. Therefore, each column of inclusions in the y-direction can properly be modeled as a solenoid with the magnetic field given by (2).

In an artificial medium, the effective magnetic susceptibility, the degree of magnetization of the medium in response to an applied magnetic field is defined as

$$\chi_{m_{\rm eff}} = \frac{M}{H_{\rm ext}} \tag{3}$$

where M is the magnitude of $\mathbf{M}$, the magnetization vector of the medium. Magnetization is defined as the magnetic moment per unit volume. In this case, the magnetic dipole moments are in phase with the external magnetic field yielding a magnetized medium where the effective magnetic susceptibility is larger than zero (or the effective permeability is larger than unity).

The magnetic dipole moment of inclusions can be simply derived as[1]

$$m_{\rm incl} = nIs. \tag{4}$$

To derive an explicit relation for the magnetic susceptibility based on physical and geometrical characteristics of the inclusion-filled medium, we propose a circuit model for the inclusions. Accordingly, the induced $V_{\rm emf}$ dropped over any inclusion can be expressed by the impedance of the rings and the induced current on the inclusion as [5]

$$V_{\rm emf} = I\left(R + \frac{1}{j\omega C}\right) \tag{5}$$

where the effective impedance of the loops has been modeled with a resistor, R, in series with a capacitor, C. The skin depth of the conductor determines the relationship between the resistance and the frequency. Therefore, R is given by:

$$R = \frac{1}{\delta\sigma}\left(\frac{n'l}{b}\right) = \frac{n'l}{b}\left(\sqrt{\frac{\mu_0\omega}{2\sigma}}\right) = R_0 l\sqrt{\omega} \tag{6}$$

where n' is the number of wire turns which contribute to ohmic losses [$n' = 2$ for case (a), (b) and (c)], and R_0 is

$$R_0 = \frac{n'}{b}\left(\sqrt{\frac{\mu_0}{2\sigma}}\right)$$

The relative permeability of the conductor in (6) was considered to be 1. Also, C is given by

$$C = C_0 l \tag{7}$$

$R_0\sqrt{\omega}$, and C_0 are defined as the per-unit-length resistance and the per-unit-length capacitance of the inclusion. The per-unit-length capacitance, for the edge-coupled inclusion can be expressed as [22]

$$C_0 = \epsilon_0\epsilon_r \frac{F\left(\sqrt{1-u^2}, \frac{\pi}{2}\right)}{F\left(u, \frac{\pi}{2}\right)}, \quad u = \frac{g}{2b+g} \tag{8}$$

and for the broadside-coupled inclusion as [5]

$$C_0 = \frac{1}{4}\epsilon_0\epsilon_r \frac{F\left(u, \frac{\pi}{2}\right)}{F\left(\sqrt{1-u^2}, \frac{\pi}{2}\right)}, \quad u = \tanh\left(\frac{\pi b}{2g}\right) \tag{9}$$

where ϵ_r is the relative permittivity of the host substrate, and $F(k, \phi)$ is the elliptical integral of the first kind

$$F(k,\phi) = \int_0^{\phi} \frac{d\theta}{\sqrt{1 - k^2\sin^2\theta}}. \tag{10}$$

It is worth noticing that in the case of *metasolenoid* [5] the gap, g, between the parallel inclusions is equal to the unit cell height, δy.

Equating (1) and (5), and using (3) and (4), the effective magnetic susceptibility can be expressed as

$$\begin{aligned}\chi_{m_{\rm eff}} &= -\frac{s}{A}\left(\frac{j\omega L}{R + j\omega L + \frac{1}{j\omega C}}\right) \\ &= \frac{s}{A}\left(\frac{\omega^2 LC}{1 - \omega^2 LC + j\omega RC}\right)\end{aligned} \tag{11}$$

where the inductance,L, is defined as

$$L = \left(\frac{n^2\mu_0}{\delta y}\right)s = L_0 s \tag{12}$$

and L_0 is the per-unit-area inductance of the inclusion.

[1]In previous works [5], [8] the magnetic dipole moment was incorrectly expressed as $m_{\rm incl} = \mu_0 nIs$.

Authorized licensed use limited to: University of Waterloo. Downloaded on July 21,2010 at 14:45:05 UTC from IEEE Xplore. Restrictions apply.

Substituting the resistance, inductance and capacitance from (6), (7) and (12) in (11) results in an expression for the net magnetic susceptibility as a function of the geometrical and physical properties of the contour Γ

$$\chi_m(\omega) = \frac{1}{A}\left(\frac{L_0C_0\omega^2 s^2 l}{1 - L_0C_0\omega^2 sl + jR_0C_0\omega\sqrt{\omega}\, l^2}\right). \quad (13)$$

As observed in (13), the susceptibility is related to the perimeter l and area s of the contour. Thus, inclusions with different topologies but having the same perimeter and area, result in the same values for the magnetic susceptibility and permeability (assuming all other physical parameters remain constant). Equation (13) can be rewritten as

$$\chi_m(\omega; s, l) = \frac{\left(\frac{\omega}{\omega'_0}\right)^2 \left(\frac{s}{A}\right) sl}{1 - \left(\frac{\omega}{\omega'_0}\right)^2 sl + j\left(\frac{\omega}{\omega''_0}\right)^{3/2} l^2} \quad (14)$$

where ω'_0, ω''_0 are defined as

$$\omega'^2_0 = \frac{1}{L_0C_0}, \quad \omega''^3_0 = \frac{1}{(R_0C_0)^2}.$$

The circumference and area of the contour, however, are not independent parameters. They are related according to the following relation:

$$\omega_0 = \frac{1}{\sqrt{LC}} = \frac{1}{\sqrt{L_0C_0sl}}. \quad (15)$$

Hence

$$sl = \left(\frac{\omega'_0}{\omega_0}\right)^2 \quad (16)$$

where the frequency ω_0 is considered as the resonance frequency of the artificial magnetic medium.

Considering (16), grouping all the physical parameters into one parameter P, and defining Ω as the normalized frequency (with respect to the resonance frequency ω_0) (14) can be rewritten as

$$\chi_m(\Omega; F, P) = \frac{F\Omega^2}{1 - \Omega^2 + jPF^{-2}\sqrt{\Omega^3}} \quad (17)$$

where $\Omega = \omega/\omega_0$ and F is the fractional area of the cell occupied by the interior of the inclusion given by

$$F = \frac{s}{\delta x\, \delta z} = \frac{s}{A} \quad (18)$$

and P is defined as

$$P = \frac{1}{A^2}\frac{{\omega'_0}^4}{\sqrt{\omega_0{}^5{\omega''_0}^3}}. \quad (19)$$

Using (17), the effective permeability can be written as

$$\begin{aligned}\mu(\Omega; F, P) &= 1 + \chi_m(\Omega; F, P) \\ &= 1 + \frac{F\Omega^2}{1 - \Omega^2 + jPF^{-2}\sqrt{\Omega^3}}. \end{aligned} \quad (20)$$

In (19), P depends on the resonance frequency ω_0, as well as the physical properties of the design such as the permittivity of the host substrate, ϵ_r, width of the metal strips, b, and space between the strips, g, (in edge-coupled inclusions) or gap, g, between parallel contours in a unit cell (in broadside-coupled inclusion) and the resistance. By factoring the frequency-related parts, the physical parameter P can be expressed as

$$P = \mathcal{K}\omega_0{}^{-\frac{5}{2}} \quad (21)$$

where $\mathcal{K}$ is related only to the physical parameters (conductivity of inclusion, width and height of route of an inclusion, and permittivity of host medium), and is expressed as

$$\mathcal{K} = \frac{R_0}{A^2{L_0}^2C_0} = \frac{n'(\delta y)^2}{n^4(\delta x)^2(\delta z)^2 b\sqrt{2\mu_0{}^3\sigma}C_0(\epsilon_r, g, b, t)}. \quad (22)$$

Note that P is expressed as the multiplication of a frequency-invariant coefficient, $\mathcal{K}$ and a simple function of the resonance frequency which is typically specified in a given design problem.

As a summary, we have derived generalized expressions for the permeability and susceptibility governing the behavior of composite engineered magnetic materials with any arbitrary shape of inclusion. To generalize the expression for use in any frequency range, it is expressed in terms of the normalized angular frequency Ω. Therefore, for any structure, calculations of P and F are sufficient to obtain the effective magnetic behavior.

III. Fundamental Limitations on Frequency Dispersion

Artificial magnetic materials are designed to provide enhanced positive permeability over a specific range of frequencies. For most of applications, it is desirable to have a uniform permeability over the range of frequencies of interest, however, due to the resonating nature of inclusions, the permeability resulting from engineered magnetic materials changes rapidly with frequency [4], [5]. The variation with frequency will result in dispersion leading to limited if not poor performance in many applications related to antenna miniaturization and gain enhancement [15]. In this section, the fundamental limitations on frequency dispersion reduction in the design of artificial magnetic materials are investigated for the lossless case where the conductivity of the conductor is assumed infinite and for the case where Ohmic losses are present.

A. Lossless Case

A typical response of an artificial magnetic medium is shown in Fig. 3. By assuming zero resistance in the metallic inclusions, the resultant susceptibility of the lossless case, χ_0 from (14) and (16) will be a real number and is equal to

$$\chi_{m0}(\omega) = \frac{\left(\frac{\omega}{\omega_0}\right)^2 F}{1 - \left(\frac{\omega}{\omega_0}\right)^2} \quad (23)$$

Assuming ω_1 and ω_2 as the lowest and highest operational frequencies $(\omega_1 < \omega_2)$, and μ_1, μ_2 as the resultant permeability at these frequencies respectively, we are seeking a general relationship between, $\delta\mu = \mu_2 - \mu_1$, and, $BW = \omega_2 - \omega_1$. (Since

Authorized licensed use limited to: University of Waterloo. Downloaded on July 21,2010 at 14:45:05 UTC from IEEE Xplore. Restrictions apply.

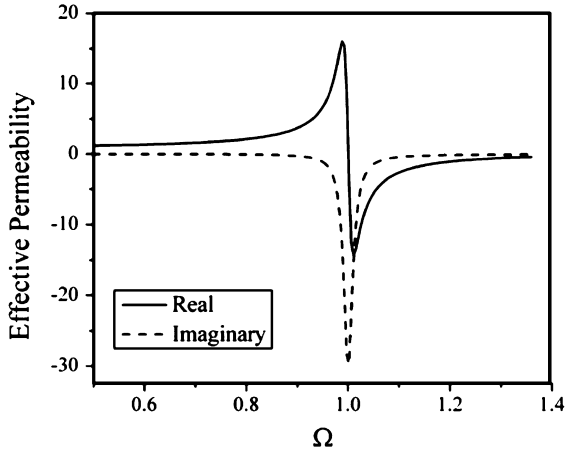

Fig. 3. A typical response of an artificial magnetic medium showing the effective permeability as a function of normalized frequency.

the engineered magnetic materials are designed to provide permeability higher than one, the frequencies ω_1 and ω_2, are chosen to be less than the resonance frequency ω_0.)

Enforcing (23) at ω_1 and ω_2 we have

$$\begin{cases} \chi_1 = \dfrac{F\left(\frac{\omega_1}{\omega_0}\right)^2}{1-\left(\frac{\omega_1}{\omega_0}\right)^2} \\ \chi_2 = \dfrac{F\left(\frac{\omega_2}{\omega_0}\right)^2}{1-\left(\frac{\omega_2}{\omega_0}\right)^2} \end{cases}. \tag{24}$$

Solving the system of equations (24) for F yields

$$F = \frac{\left({\omega_2}^2-{\omega_1}^2\right)(\chi_2\chi_1)}{\chi_2{\omega_1}^2 - \chi_1{\omega_2}^2}. \tag{25}$$

Recall that since F is the fractional area occupied by the interior of the inclusion in the unit cell, F is bound by unity. Satisfying the conditions of $0 < F < 1$ leads to restrictions on the susceptibilities at two selected frequencies. For the first condition $F > 0$, it is clear that the permeability is larger than one and therefore the susceptibility is positive for all frequencies less than ω_0, (i.e., $\mu_2, \mu_1 > 1$ and $\chi_2, \chi_1 > 0$). Consequently, since $\omega_2 > \omega_1$, we have

$$\left(\frac{\omega_2}{\omega_1}\right)^2 \leq \frac{\chi_2}{\chi_1}. \tag{26}$$

The above equation shows an interesting constraint which limits the ratio of the susceptibility at any two arbitrary frequencies to the square of the ratio of those frequencies. Another interesting observation is that the relationship given in (26) is independent of both physical and geometrical characteristics of the designed inclusion. Any effort to improve the frequency bandwidth of the resultant permeability is strictly confined to this limitation. As an example, suppose $\omega_2 = 3\omega_1$, then χ_2/χ_1 cannot be less than 9.

For the second condition, namely, $F < 1$, we consider (25) and after some algebraic manipulations, we have

$$\left(\frac{\omega_2}{\omega_1}\right)^2 \leq \left(\frac{\chi_2}{\chi_1}\right)\left(\frac{\chi_1+1}{\chi_2+1}\right). \tag{27}$$

or equivalently

$$\left(\frac{\omega_2}{\omega_1}\right)^2 \leq \left(\frac{\chi_2}{\chi_1}\right)\left(\frac{\mu_1}{\mu_2}\right). \tag{28}$$

Since the ratio of $(\chi_1+1)/(\chi_2+1)$ is always less than one, the limit achieved in (28) is even stronger than that of (26). Therefore, the change of susceptibility with frequency is even more rapid than the square of frequency.

By defining mean permeability μ_c and central frequency ω_c, respectively, as

$$\mu_c = \frac{1}{2}(\mu_2+\mu_1)$$
$$\omega_c = \frac{1}{2}(\omega_2+\omega_1)$$

and $\delta\chi$ and $\delta\mu$ as the deviation of susceptibility and permeability, respectively, (28) can be rewritten as

$$\left(\frac{\chi_c+\frac{\delta\chi}{2}}{\chi_c-\frac{\delta\chi}{2}}\right)\left(\frac{\mu_c-\frac{\delta\mu}{2}}{\mu_c+\frac{\delta\mu}{2}}\right) \geq \left(\frac{\omega_c+\frac{\mathrm{BW}}{2}}{\omega_c-\frac{\mathrm{BW}}{2}}\right)^2. \tag{29}$$

In many application $\mathrm{BW} \ll \omega_c$ and $\delta\mu \ll \mu_c$. Using these conditions, (29) can be simplified using first-order binomial expansions as

$$\begin{cases} \left(\frac{\omega_2}{\omega_1}\right)^2 = \left(\frac{\omega_c+\frac{\mathrm{BW}}{2}}{\omega_c-\frac{\mathrm{BW}}{2}}\right)^2 \cong 1+\frac{2\mathrm{BW}}{\omega_c} \\ \left(\frac{\chi_2}{\chi_1}\right)\left(\frac{\mu_1}{\mu_2}\right) = \left(\frac{\chi_c+\frac{\delta\chi}{2}}{\chi_c-\frac{\delta\chi}{2}}\right)\left(\frac{\mu_c-\frac{\delta\mu}{2}}{\mu_c+\frac{\delta\mu}{2}}\right) \\ \quad \cong \left(1+\frac{\delta\chi}{\chi_c}\right)\left(1-\frac{\delta\mu}{\mu_c}\right) \\ \cong 1+\delta\mu\left(\frac{1}{\chi_c}-\frac{1}{\mu_c}\right) = 1+\frac{\delta\mu}{\chi_c\mu_c} \end{cases}. \tag{30}$$

Substituting (30) in (28) results in

$$\frac{\mathrm{BW}}{\omega_c} \leq \frac{1}{2\chi_c}\left(\frac{\delta\mu}{\mu_c}\right). \tag{31}$$

The condition in (31) relates the deviation in the relative permeability to the relative bandwidth. Since the bandwidth BW is inversely proportional to the mean permeability μ_c, there is a tradeoff between maximizing the effective permeability and broadening the frequency range in which the smooth deviation of permeability is obtainable. In fact, for two different designs with the same relative permeability deviation, wider bandwidth can be achieved in the design with lower permeability.

Fig. 4 illustrates (31) graphically. For any design, the resultant bandwidth lies in the gray area shown in Fig. 4. As an example, for μ_c equal to 5, requiring the relative permeability deviation to be less than 1 percent bounds the relative frequency bandwidth to 0.125%, and say, for a central frequency of 200 MHz the bandwidths would theoretically be less than 250 kHz. As a second example, if $\mu_c = 2$, having 1% deviation in the permeability leads to a maximum of 0.5% relative bandwidth.

Although first-order terms were used in the Taylor's expansion in (31), it can be shown that making the approximation more accurate by including second-order terms in the expansion gives identical conclusions.

B. Lossy Case

By considering loss, the resultant permeability in (20) or the resultant susceptibility in (17) will have real and imaginary parts. Since only the real part affects the permeability in the

Authorized licensed use limited to: University of Waterloo. Downloaded on July 21,2010 at 14:45:05 UTC from IEEE Xplore. Restrictions apply.

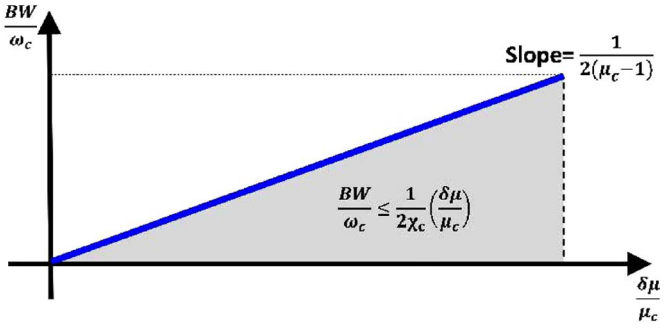

Fig. 4. The relative frequency bandwidth is depicted versus the relative permeability deviation. The gray area determines the possible interval for the bandwidth. Notice that the slope is inversely proportional to the central susceptibility.

artificial magnetic medium and the imaginary part appears only when introducing loss in the medium, the deviation with frequency is mostly important for the real part.

In this section we study the frequency deviation of the real part only, and in the next section the magnitude of the imaginary part and methods and limitations to decrease it will be discussed.

As shown in Section I, the resultant permeability can be modeled as the response of an RLC circuit. It is expected that adding resistance or loss to the system (inclusions) leads to a smoother frequency response. Therefore, it is expected that the fundamental limits achieved for the frequency response of the permeability in Subsection III.A for the lossless case to be sufficient for the lossy case. To show this, we consider the real part of (17) as the resultant magnetic susceptibility of the medium. The real part of the magnetic susceptibility is given by

$$\chi_{m\mathrm{Re}}(\Omega;F,P) = \mathcal{R}e(\chi_m(\Omega;F,P)) = \frac{F^5\Omega^2(1-\Omega^2)}{F^4(1-\Omega^2)^2+P^2\Omega^3}. \tag{32}$$

Using (23), the real part can be expressed in term of the susceptibility of the lossless case, χ_{m0} as

$$\chi_{m\mathrm{Re}}(\Omega;F,P) = \frac{F\Omega^2}{1-\Omega^2}\left\{\frac{1}{1+\frac{P^2\Omega^3}{F^4(1-\Omega^2)^2}}\right\} = \chi_{m0}\left\{\frac{1}{1+\xi(\Omega)}\right\} \tag{33}$$

where $\xi(\Omega)$ is defined as

$$\xi(\Omega) = \frac{P^2\Omega^3}{F^4(1-\Omega^2)^2} = \alpha^2\frac{\Omega^3}{(1-\Omega^2)^2} \tag{34}$$

and $\alpha = P/F^2$.

The factor α determines the level of loss in the medium and therefore we call it the *dissipation factor*. Since frequencies below the resonance frequency result in permeability higher than one, the frequency range $0 < \Omega < 1$ is considered to be the only frequency range of relevance when designing artificial magnetic permeability that achieves enhanced positive permeability. Therefore, in the context of this work, we focus our attention on this range only.

The function $\xi(\Omega)$ has a second-order simple singularity at the normalized resonance frequency (i.e., $\Omega = 1$), thus $\xi(\Omega)$ approaches infinity as Ω approaches one. The factor α in (34) is a parameter that scales the magnitude of $\xi(\Omega)$ and all its derivatives. Differentiation of $\xi(\Omega)$ with respect to Ω gives

$$\frac{d\xi(\Omega)}{d\Omega} = \alpha^2\frac{\Omega^2(3+\Omega^2)}{(1-\Omega^2)^3}. \tag{35}$$

In the range $0 < \Omega < 1$, (35) is always positive, therefore, the function increases monotonically with respect to Ω. So, for $\Omega_2 > \Omega_1$, we have

$$\xi(\Omega_2) \geq \xi(\Omega_1). \tag{36}$$

Using (36), (33) leads to

$$\frac{\chi_{m0}(\Omega_1)-\chi_{m\mathrm{Re}}(\Omega_1)}{\chi_{m\mathrm{Re}}(\Omega_1)} \leq \frac{\chi_{m0}(\Omega_2)-\chi_{m\mathrm{Re}}(\Omega_2)}{\chi_{m\mathrm{Re}}(\Omega_2)}. \tag{37}$$

Simplification of (37) results in

$$\frac{\chi_{m\mathrm{Re}}(\Omega_2)}{\chi_{m\mathrm{Re}}(\Omega_1)} \leq \frac{\chi_{m0}(\Omega_2)}{\chi_{m0}(\Omega_1)}. \tag{38}$$

The inequality in (38) states that the ratio of the magnetic susceptibility at two different frequencies for the lossless case is larger than that of the lossy case. This indicates that the magnetic susceptibility function is flatter for the lossy case than for the lossless case. Note that the limit achieved in (31) is independent of the topology of the inclusion.

IV. The Effect of Physical and Geometrical Parameters on Dispersion and Loss

As shown in Section II, all physical properties can be summarized in one parameter, P, and all geometrical properties can be summarized in one parameter F. Equation (33) gives the magnetic susceptibility and consequently the permeability in terms of these two parameters, P and F. Therefore, the study of the effect of physical and geometrical parameters on the resultant permeability and its frequency domain behavior will be confined to F and P.

A. Real Part of Permeability

Differentiation of (36) with respect to F gives

$$\frac{\partial\mu_{\mathrm{Re}}(\Omega;F)}{\partial F} = \frac{\partial\chi_{\mathrm{Re}}(\Omega;F)}{\partial F} = \frac{\Omega^2(1-\Omega^2)\left((1-\Omega^2)^2+5P^2F^{-4}\Omega^3\right)}{\left((1-\Omega^2)^2+P^2\Omega^3F^{-4}\right)^2} = \frac{\Omega^2}{1-\Omega^2}\left(\frac{1+5\xi(\Omega)}{1+\xi(\Omega)}\right). \tag{39}$$

In the frequency range of interest, $0 < \Omega < 1$, we have

$$\frac{\partial\mu_{\mathrm{Re}}(\Omega;F)}{\partial F} > 0. \tag{40}$$

Authorized licensed use limited to: University of Waterloo. Downloaded on July 21,2010 at 14:45:05 UTC from IEEE Xplore. Restrictions apply.

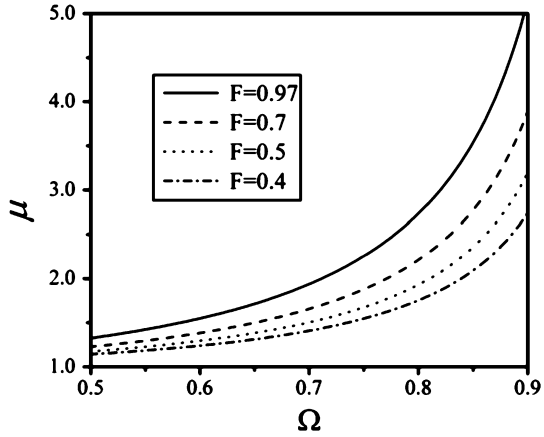

Fig. 5. Real part of the permeability as a function of the normalized frequency, Ω, for different values of F. The inclusion trace is made of copper and the dimensions are similar to those reported in [8]: $g = b = 0.127$ mm, $\varepsilon_r = 3.38$, $\delta y = 3.028$ mm, $\delta x = \delta z = 20$ mm.

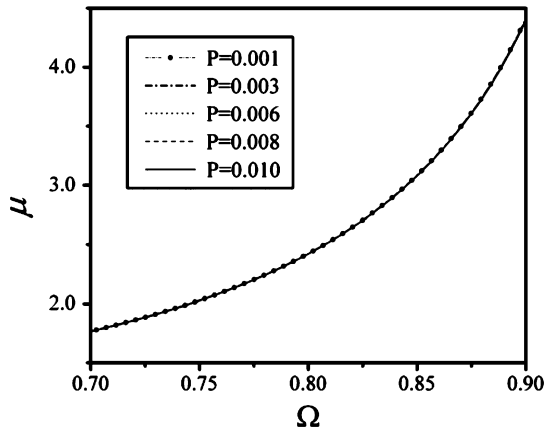

Fig. 6. The real part of permeability for different values of P, the geometrical parameter F is assumed to be 0.8. Notice that all curves are almost overlapping.

Therefore, the larger F, the higher the permeability. Since F is defined as the ratio of the surface enclosed by the inclusion to the total surface of the unit cell, the contours which provide higher enclosed surface lead to higher permeability. On the other hand, the surface of the inclusion and its length are related to each other through the resonance frequency in (15). Indeed, they are inversely proportional at a fixed resonance frequency. Therefore, for all inclusions designed to operate at the same resonance frequencies, the ones that provide larger enclosed surface (or larger F) and shorter total length (i.e., perimeter) will result in higher value for permeability. Fig. 5 shows the real part of the permeability as a function of Ω for different values of F. Furthermore, Fig. 5 shows that an increase in F leads to a larger value of the permeability which is expected from (40).

Using (32), the real part of the permeability can be written as

$$\mu_{\mathrm{Re}}(\Omega) = 1 + \chi_{m\mathrm{Re}}(\Omega) = 1 + \frac{F\Omega^2}{1-\Omega^2}\left(\frac{1}{1+\xi(\Omega)}\right). \quad (41)$$

In (41), $\xi(\Omega)$ is a function of P. Taking the derivative of (41) with respect to P gives

$$\begin{aligned}\frac{\partial \mu_{\mathrm{Re}}(\Omega,P)}{\partial P} &= \frac{\partial \chi_{m\mathrm{Re}}(\Omega,P)}{\partial P} \\ &= -\frac{2}{P}\frac{F\Omega^2}{1-\Omega^2}\frac{\xi(\Omega)}{(1+\xi(\Omega))^2} \\ &= -\frac{2}{P}\frac{\xi(\Omega)}{1+\xi(\Omega)}\chi_{m\mathrm{Re}}(\Omega;F). \end{aligned} \quad (42)$$

Notice that (42) is always negative for $0 < \Omega < 1$. Therefore, by increasing P, we expect the permeability to decrease. However, what is interesting is that for practical considerations, μ is highly insensitive to changes in P. Fig. 6 shows a plot of μ vs. Ω, for the case of $F = 0.8$ (this case was simply selected as an example). We observe that as P changes by one order of magnitude, the resultant permeability remains practically constant. Notice that the curves in Fig. 6 are indistinguishable. This is due to the fact that in (41), the only part that is a function of P is $\xi(\Omega)$ which is much smaller than 1. (Since $\alpha = P/F^2$, and from (34), it can be shown that for practical geometries such as those considered in Table I, $\xi(\Omega) \ll 1$. Notice that we are assuming that the upper frequency of interest is not close to the resonance frequency. As the resonance frequency is approached, the curves in Fig. 7 start to diverge and $\xi(\Omega)$ is no longer much smaller than one.)

Table I shows three P values for designs proposed earlier in the literature. In all cases, the P factor was small, even in some cases smaller than the numbers we considered for the graph in Fig. 6.

B. Magnetic Loss Tangent

An important parameter in designing artificial magnetic materials is the *Magnetic Loss Tangent*, $\tan\delta$, which represents the magnetic loss in the medium. In most applications, it is desirable to have $\tan\delta$ as small as possible. In this section, the behavior of $\tan\delta$ with respect to the geometrical and physical parameters, F and P, is investigated.

The magnetic loss tangent is defined as

$$\tan\delta = -\frac{\mathcal{I}m(\mu(\omega))}{\mathcal{R}e(\mu(\omega))}. \quad (43)$$

Using (20), $\tan\delta$ can be rewritten as

$$\tan\delta = \frac{F\Omega^2\sqrt{\xi(\Omega)}}{(1+\xi(\Omega))(1-\Omega^2)+F\Omega^2}. \quad (44)$$

Differentiating (44) with respect to F, we obtain

$$\frac{\partial(\tan\delta)}{\partial F} = -\frac{\Omega^2(1-\Omega^2)(1-3\xi(\Omega))\sqrt{\xi(\Omega)}}{\left((1+\xi(\Omega))(1-\Omega^2)+F\Omega^2\right)^2}. \quad (45)$$

In (45), all terms except $(1-3\xi(\Omega))$, are positive for all values of F and Ω. Since $\xi(\Omega)$ is inversely related to F [see (34)], $\tan\delta$ has a local maximum at a specific value of F denoted as $F_{\max}$. In Fig. 7, $\tan\delta$ is plotted as a function of F for different values of P and Ω. Notice that, $F_{\max}$, the value of F corresponding to maximum $\tan\delta$, is relatively small compared to unity, meaning that $\tan\delta$ reaches a maximum when the area of the inclusions is small in comparison to the area of the unit cell. Since the permeability approaches unity for small values of F, it is most desirable to achieve the highest permeability, hence, F is chosen to be greater than $F_{\max}$.

Authorized licensed use limited to: University of Waterloo. Downloaded on July 21,2010 at 14:45:05 UTC from IEEE Xplore. Restrictions apply.

TABLE I
PARAMETERS OF SOME PREVIOUSLY DESIGNED INCLUSIONS

Design	$A(mm^2)$	$\mathcal{K}$	$\omega_0(GHz)$	P	F
Solenoid [5]	110	2.3×10^{19}	0.998	9.8×10^{-6}	0.11
SRR [4]	100	9.0×10^{21}	32.58	4.9×10^{-4}	0.53
Hilbert-SRR [8]	400	7.5×10^{19}	0.981	2.4×10^{-2}	0.42

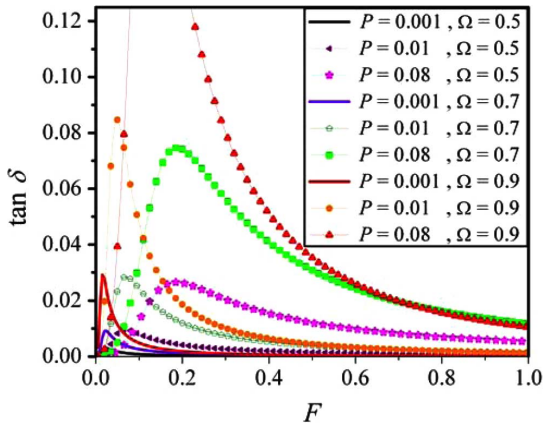

Fig. 7. The magnetic loss tangent, $\tan\delta$, as a function of the geometrical parameter, F, for different values of P and Ω.

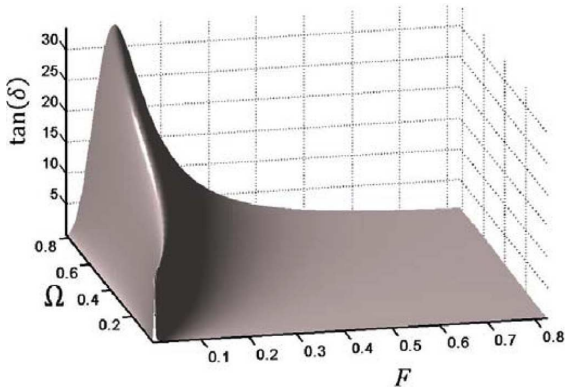

Fig. 8. The magnetic loss tangent, $\tan\delta$, as a function of Ω and F, for $P = 0.05$.

For designs with F larger than $F_{\max}$, as shown in Fig. 7, increasing F leads to a smaller value of $\tan\delta$. Consequently, an optimal design is a design with inclusions whose area is close to the unit cell's area $(F \to 1)$ which leads to a lower magnetic loss. Hence, the minimum value of $\tan\delta$, achieved at $F = 1$, is

$$\min(\tan\delta) = \tan\delta|_{F=1} \cong \Omega^2\sqrt{\xi(\Omega)} = \frac{\sqrt{\Omega^7}}{1-\Omega^2}P. \quad (46)$$

Fig. 8 shows a three dimensional presentation of $\tan\delta$ as a function of F and Ω. As shown in this figure, the maximum value of $\tan\delta$ occurs at the lower value of F. For instance, for an inclusion with a physical factor P less than 0.002, the maximum of $\tan\delta$ at any frequency occurs at F less than 0.2. Moreover, as F increases, i.e., the inclusion occupies more area of the unit cell, the maximum moves to larger Ω and also becomes larger (from about 10 when Ω and F are close to zero, and more than 35 when Ω is 0.8 and F is 0.1). In addition, it can be observed that as F approaches unity $\tan\delta$ decreases.

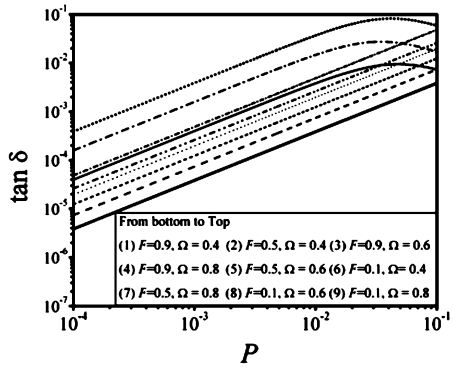

Fig. 9. The magnetic loss tangent $\tan\delta$ as a function of the physical parameter, P for different values of F and Ω.

To study the effect of physical parameters on loss, we need to consider the derivative of $\tan\delta$ with respect to P

$$\frac{\partial(\tan\delta)}{\partial P} = \frac{F\Omega^2\sqrt{\xi(\Omega)}((1-\xi(\Omega))(1-\Omega^2)+F\Omega^2)}{P((1+\xi(\Omega))(1-\Omega^2)+F\Omega^2)^2}. \quad (47)$$

For a specific value of P, denoted as $P_{\max}$, the term $(1-\xi(\Omega)(1-\Omega^2)+F\Omega^2)$ vanishes, and $\tan\delta$ reaches a maximum for a certain value of F and Ω. (It is a simple exercise to show that $\tan\delta$ has only one maximum within the range of P. In Fig. 9, $\tan\delta$ is plotted as a function of P for different values of F and Ω. As shown in Fig. 9, the maximum of $\tan\delta$ function occurs for values of P much higher than those used in practical structures.

V. CONCLUSION

In this work, we presented fundamental limitations on the performance of artificial magnetic materials. The formulation is based on a circuit model that incorporates the physical behavior of the inclusion. The permeability and magnetic susceptibility of the media were formulated in terms of a *geometrical* parameter, F, that represents the geometrical characteristics of the inclusions such as area, perimeter and curvature, and a *physical* parameters, P, that represents the physical, structural and fabrication characteristics of the medium. Fundamental constraints expressing the effect of the relative permeability on the relative bandwidth were derived for the lossless and lossy structures. It is shown that the achieved restriction is general and does not depend on the shape of the metallic inclusions comprising the artificial magnetic medium.

Authorized licensed use limited to: University of Waterloo. Downloaded on July 21,2010 at 14:45:05 UTC from IEEE Xplore. Restrictions apply.

The effect of the physical and geometrical parameters, P and F, respectively, on the effective permeability of the medium and the magnetic loss tangent were studied. It was found that increasing F increases the effective permeability of the medium, however, it also leads to increased dispersion. Increasing the geometrical factor F was found to decrease the loss. It was also found that the physical parameter, P has very little impact on the effective permeability and dispersion; however, it affects the loss more pronouncedly. Therefore, there is a tradeoff between increasing the permeability and decreasing the loss on the one hand, which results from increasing F, and reducing dispersion, on the other hand by decreasing F. In other words, designing inclusions with larger surface area (i.e., increasing F) results in lower loss and higher value for permeability; however, this leads to an increase in the rate of change of permeability with frequency, thus higher dispersion.

The constraints and relations derived in this work can be used to methodically design artificial magnetic material meeting specific operational requirements.

REFERENCES

[1] S. B. Narang and I. S. Hudiara, "Microwave dielectric properties of m type barium, calcium and strontium hexaferrite substituted with co and ti," *J. Ceramic Processing Res.*, vol. 7, no. 2, pp. 113–116, 2006.

[2] W. D. Callister, *Materials Science and Engineering, an Introduction*. New York: Wiley, 2000.

[3] M. V. Kostin and V. V. Shevchenko, "Artificial magnetics based on double circular elements," in *Proc. Bian-Isotropics'94*, Perigueux, France, May 1994, pp. 49–56.

[4] J. B. Pendry, A. J. Holden, D. J. Robbins, and W. J. Stewart, "Magnetism from conductors and enhanced nonlinear phenomena," *IEEE Trans. Microw. Theory Tech.*, vol. 47, no. 11, pp. 2075–2084, Nov. 1999.

[5] S. Maslovski, P. Ikonen, I. Kolmakov, and S. Tretyakov, "Artificial magnetic materials based on the new magnetic particle: Metasolenoid," *Progr. Electromagn. Res. (PIER)*, vol. 54, no. 9, pp. 61–81, Sept. 2005.

[6] R. Marques, F. Medina, and R. Rafii-El-Idrissi, "Role of bianisotropy in negative permeability and left-handed metamaterials," *Phys. Rev. B*, vol. 65, no. 14, pp. 44 401–44 404, Nov. 2002.

[7] J. D. Baena, R. Marques, and F. Medina, "Artificial magnetic metamaterial design by using spiral resonators," *Phys. Rev. B*, vol. 69, pp. 144 021–144 025, Jan. 2004.

[8] L. Yousefi and O. M. Ramahi, "New artificial magnetic materials based on fractal Hilbert curves," in *Proc. IWAT07*, 2007, pp. 237–240.

[9] B. Sauviac, C. R. Siovski, and S. A. Tretyakov, "Double split-ring resonators: Analytical modeling and numerical simulation," *Electromagnetics*, vol. 24, no. 5, pp. 317–338, 2004.

[10] A. Ishimaru, S. Lee, Y. Kuga, and V. Jandhyala, "Generalized constitutive relations for metamaterials based on the quasi-static lorentz theory," *IEEE Trans. Antennas Propag.*, vol. 51, no. 10, pp. 2550–2557, Oct. 2003.

[11] D. R. Smith and J. B. Pendry, "Homogenization of metamaterials by field averaging," *J. Opt. Soc. Am. B*, vol. 23, no. 3, pp. 391–403, Mar. 2006.

[12] M. G. Silveirinha, "Metamaterial homogenization approach with application to the characterization of microstructured composites with negative parameters," *Phys. Rev. B*, vol. 75, pp. 1–15, 2007, 115104.

[13] M. Shamonin, E. Shamonina, V. Kalinin, and L. Solymar, "Properties of a metamaterial element: Analytical solutions and numerical simulations for a singly split double ring," *J. Appl. Phys.*, vol. 95, no. 57, pp. 3778–3784, 2004.

[14] P. Ikonen and S. A. Tretyakov, "Determination of generalized permeability function and field energy density in artificial magnetics using the equivalent-circuit method," *IEEE Trans. Antennas Propag.*, vol. 55, no. 1, pp. 92–99, 2007.

[15] P. Ikonen, S. I. Maslovski, C. R. Simovski, and S. A. Tretyakov, "On artificial magnetodielectric loading for improving the impedance bandwidth properties of microstrip antennas," *IEEE Trans. Antennas Propag.*, vol. 54, no. 6, pp. 1654–1662, Jun. 2006.

[16] K. Buell, H. Mosallaei, and K. Sarabandi, "A substrate for small patch antennas providing tunable miniaturization factors," *IEEE Trans. Microw. Theory Tech.*, vol. 54, pp. 135–146, Jan. 2006.

[17] M. Boybay and O. M. Ramahi, "Near-field probes using double and single negative media," in *Proc. NATO Advanced Res. Workshop: Metamaterials for Secure Information and Communication Technologies*, May 2008, vol. 1B, pp. 725–731.

[18] G. Lovat and P. Burghignoli, "Shielding effectiveness of a metamaterial slab," in *Proc. IEEE Int. Symp. of Electromagnetic Compatibility*, Jul. 2007, vol. 1B, pp. 1–5.

[19] N. I. Landy, S. Sajuyigbe, J. J. Mock, D. R. Smith, and W. J. Padillal, "Perfect metamaterial absorber," *Phys. Rev. Lett.*, vol. 100, no. 20, pp. 207–402, May 2008.

[20] F. Bilotti, A. Alu', N. Engheta, and L. Vegni, "Features of a metamaterial based microwave absorber," in *Proc. the Workshop on Metamaterials and Special Materials for Electromagnetic Applications and TLC*, Rome, Italy, Mar. 2006, vol. 1B, pp. 11–14.

[21] S. A. Cummer, B.-I. Popa, and T. H. Hand, "Q-based design equations and loss limits for resonant metamaterials and experimental validation," *IEEE Trans. Antennas Propag.*, vol. 56, no. 1, pp. 127–132, Jan. 2008.

[22] R. Schinzinger and P. Laura, *Conformal Mapping: Methods and Applications*. The Netherlands: Elsevier, 1991.

Ali Kabiri was born in Tehran, Iran, in 1978. He received the B.Sc. degree in electrical engineering from Sharif University of Technology, Tehran, Iran, in 2000 and the M.Sc. degree in theoretical physics and elementary particles (highest honors) from the University of Tehran, Tehran, in 2002.

From 2002 to 2006, He was a Manager at SAM Electronics (subsidiary of Samsung), Tehran. Currently, he is working toward the Ph.D. degree at the University of Waterloo, Waterloo, ON, Canada. His research interests include metamaterials, artificial magnetic materials, nano-plasmonics, and optical magnetism.

Leila Yousefi was born in Isfahan, Iran, in 1978. She received the B.Sc. and M.Sc. degrees in electrical engineering from Sharif University of Technology, Tehran, Iran, in 2000, and 2003, respectively, and the Ph.D. degree in electrical engineering from the University of Waterloo, Waterloo, ON, Canada, in 2009.

Currently, she is working as a Postdoctoral Fellow at the University of Waterloo. Her research interests include metamaterials, miniaturized antennas, electromagnetic bandgap structures, and MIMO systems.

Omar M. Ramahi (F'09) received dual B.S. degrees in mathematics and electrical and computer engineering (*summa cum laude*) from Oregon State University, Corvallis, in 1984, and the M.S. and Ph.D. degrees in electrical and computer engineering from the University of Illinois at Urbana-Champaign, in 1986 and 1990, respectively.

From 1990 to 1993, he held a visiting fellowship position at the University of Illinois at Urbana-Champaign. From 1993 to 2000, he worked at Digital Equipment Corporation (presently, HP), where he was a member of the Alpha Server Product Development Group. In 2000, he joined the faculty of the James Clark School of Engineering, University of Maryland at College Park, as an Assistant Professor and later as a tenured Associate Professor. At the University of Maryland, he was also a faculty member of the CALCE Electronic Products and Systems Center. Presently, he is a Professor in the Electrical and Computer Engineering Department and holds the NSERC/RIM Industrial Research Associate Chair, University of Waterloo, Ontario, Canada. He also holds cross appointments with the Department of Mechanical and Mechatronics Engineering and the Department of Physics and Astronomy. He served as a consultant to several companies and was a co-founder of EMS-PLUS, LLC and Applied Electromagnetic Technology, LLC. He has authored and coauthored over 230 journal and conference papers. He is an coauthor of the book *EMI/EMC Computational Modeling Handbook* (Springer-Verlag, 2001).

Dr. Ramahi serves as an Associate Editor for the IEEE TRANSACTIONS ON ADVANCED PACKAGING and as an IEEE EMC Society Distinguished Lecturer.

Authorized licensed use limited to: University of Waterloo. Downloaded on July 21,2010 at 14:45:05 UTC from IEEE Xplore. Restrictions apply.